X-ray Pole Figure and Small Angle Scattering Measurements on Tubular Blown Low-Density Poly(ethylene) Films

Richard J. Pazur and Robert E. Prud'homme*

Centre de recherche en sciences et ingénierie des macromolécules, Département de chimie, Université Laval, Québec, Canada G1K 7P4

Received October 12, 1994; Revised Manuscript Received August 17, 1995[⊗]

ABSTRACT: Pole figures obtained by wide-angle X-ray diffraction have been used to quantify and characterize the molecular orientations induced in low-density poly(ethylene) films prepared by the tubular film process. Small-angle X-ray scattering was employed to determine the type and orientation of the morphology within the films. All films were found to possess a combination of two morphologies: a surface transcrystalline layer and a row-nucleated morphology caused by crystallization in low-stress conditions. For the first series of blown films, in which the draw-down ratio was increased from 1.9 to 7.9 for a constant blow-up ratio of 1.68, the *a* axis was observed to increase its orientation along the extrusion direction, signifying that the row-nucleated structures intensify their orientation along this same direction. The amount of transcrystalline material decreases upon increasing the draw-down ratio. Unexpectedly, the amorphous regions tend to become biaxially oriented in the higher drawn samples. In the second series of films, the blow-up ratio was increased from 1.60 to 2.74 for a constant draw-down ratio of 4.2. In this case, the row-nucleated morphology became progressively oriented in the film plane upon bubble enlargement, thus creating an uniplanar orientation of the molecular chains in the film plane. The amorphous regions, weakly oriented on the onset along the extrusion direction, gradually become biaxially oriented in the film plane upon increasing the blow-up ratio. Finally, it was shown that molecular orientation measurements can be used to verify the consistency of the processing conditions in blown film production.

Introduction

The biaxial orientation of polymers, commonly found in sheets, films, bottles, and tubing, is a phenomenon that is extremely important for improving the mechanical, optical, thermal, and electrical properties of the large plane of the objects.[1] A deformation applied in two mutually perpendicular directions usually causes the appearance of a set of three mutually perpendicular symmetry planes, which is characteristic of a biaxially oriented sample. On a molecular scale, the polymer chains may be oriented within the specimen plane (biaxial planar) or aligned preferentially in two or more directions (bimodal, trimodal, etc.) with respect to the reference axes. In plastic processing, extrusion, or calandering followed by stretching, film blowing, or vacuum or pressure forming, blow molding may induce uni- and biaxial orientations in the end products.[2] Besides the crystal orientation, a thorough understanding of the overall morphology is necessary to predict final end-use behavior.

In semicrystalline polymers such as poly(ethylene) (PE), orientation of the molecular chains in the crystalline regions is contingent upon the morphology produced during processing. In the blown film process, the crystallization takes place under stress, causing primarily row-nucleated morphologies along extended chains or bundles oriented along the extrusion direction. The models of Keller and Machin[3] have greatly aided in the conceptual understanding of the row-nucleated morphology, especially concerning the nature of the crystal growth perpendicular to the oriented fiber-like bundles. According to their model, two major crystallizations take place depending upon the magnitude of the stress in the melt. Under low-stress conditions (Figure 1a), the lamellae grow radially outward in the form of twisted ribbons, with their growth axis parallel to the *b* crystallographic axis for PE. This crystallization process causes a preferential orientation of the *a* axis parallel to the extrusion direction (Keller/Machin 1 morphology). Under higher stresses (Figure 1b), the radially grown lamellae extend directly outward without twisting, causing the regularly folded chains within the lamellae to remain parallel to the molecular chains in the extended microfibers (Keller/Machin 2 morphology). Intermediate stresses can, in theory, give a combination of the two morphologies presented in Figure 1. Given the disposition of the lamellae in the disklike kebabs, the periodicity of the morphology is directed along the machine direction (MD). Hence, small-angle X-ray scattering (SAXS) patterns taken along the normal (ND) or transverse (TD) directions should give characteristic two-point diagrams along the MD and, thus, can verify the presence of row-nucleated structures. Furthermore, a pole figure study of the crystal orientation can easily distinguish the type of morphology (Keller/Machin 1 or 2) and assess the sort of molecular orientation present in the polymer.

The Keller/Machin 1 morphology is the most commonly observed morphology in blown PE films.[4−11,13,15] Other researchers have observed this and the combined intermediate morphology equally in LDPE and HDPE films.[4,8−14] To our knowledge, the Keller/Machin 2 morphology has been induced only in blown HDPE films.[11,12] In the present study, we analyze the crystalline molecular orientation induced in blown LDPE film by measuring the (200) and (020) pole figures. SAXS measurements will be used to ascertain the type of morphology induced in the films. By determining the orientation of the PE unit cell, it will be possible to verify the morphological models. A complete quantitative analysis will also be undertaken by way of White/Spruiell biaxial orientation functions to characterize the induced molecular orientation. An attempt will be made by way of birefringence measurements to deduce the amorphous orientation in the blown films.

[⊗] Abstract published in *Advance ACS Abstracts,* December 1, 1995.

0024-9297/96/2229-0119$12.00/0

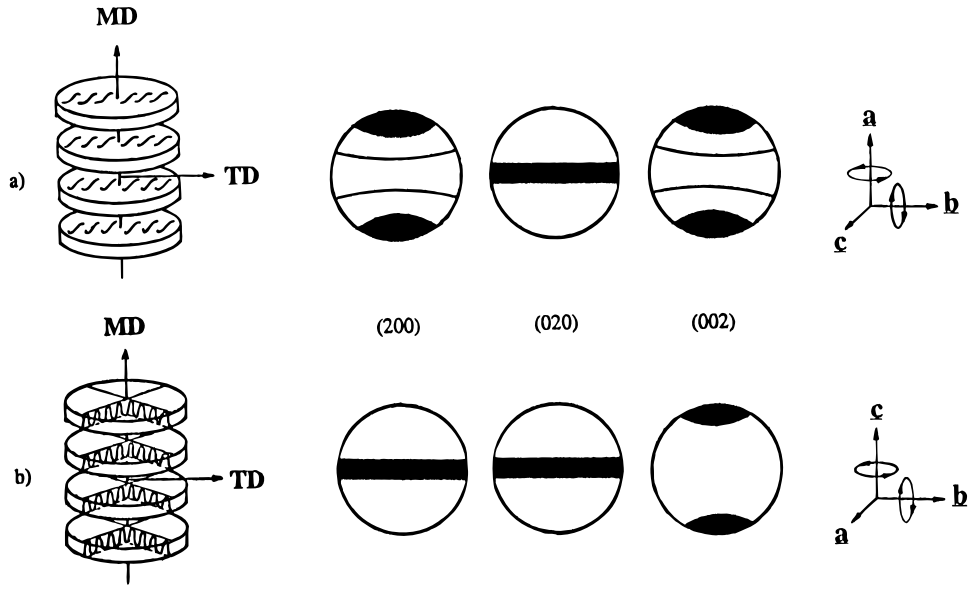

Figure 1. Morphological models of the row-nucleated structure, with predicted pole figures and unit cell orientation for PE under (a) low-stress conditions (Keller/Machin 1) and (b) high-stress conditions (Keller/Machin 2).

Theory

White and Spruiell[16] developed a series of second-moment biaxial orientation functions, which are useful for characterizing molecular orientation in films and sheets. These functions were derived by assuming a direct relationship between the second-order polarizability tensor and the second moment of the orientation distribution. Besides developing the classical Hermans orientation function, which describes uniaxial orientation states, they derived two biaxial orientation functions having the following form:

$$F_{z1}{}^{B} = 2\langle\cos^2\phi_{1x}\rangle + \langle\cos^2\phi_{1y}\rangle - 1 \qquad (1a)$$

$$F_{y1}{}^{B} = 2\langle\cos^2\phi_{1y}\rangle + \langle\cos^2\phi_{1z}\rangle - 1 \qquad (1b)$$

where B refers to biaxial orientation states. The angles ϕ_{1z} and ϕ_{1y} define one possible orientation of an axis 1 fixed to the origin of an orthogonal coordinate system *zyx* with respect to the *z* and *y* directions. The average value for all orientations of the axis is represented by the triangular brackets. Their functions characterize orientation with respect to the machine (MD or *z*) and transverse (TD or *y*) reference directions and take on the following limiting values:

1. $F_{z1}{}^{B} = 1$, $F_{y1}{}^{B} = 0$, perfect uniaxial orientation along *z*
2. $F_{z1}{}^{B} = 0$, $F_{y1}{}^{B} = 1$, perfect uniaxial orientation along *y*
3. $F_{z1}{}^{B} = -1$, $F_{y1}{}^{B} = -1$, perfect uniaxial orientation along *x*
4. $F_{z1}{}^{B} = {}^1/_2$, $F_{y1}{}^{B} = {}^1/_2$, $F_{y1}{}^{B} = {}^1/_2$, equal planar biaxial orientation

A planar orientation occurs when the polymer chains are confined in the *zy* plane, which, mathematically, corresponds to $\langle\cos^2\phi_{1x}\rangle = 0$.

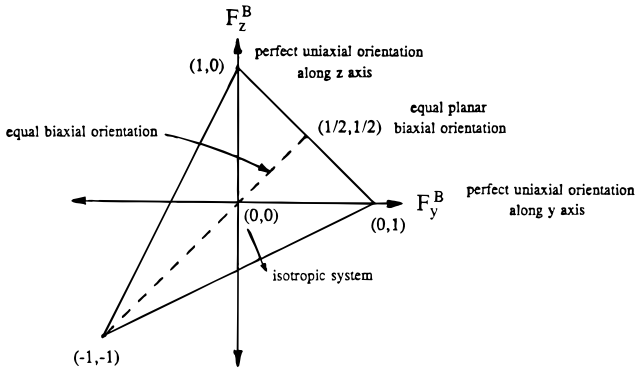

Figure 2. Biaxial orientation functions of eqs 1 plotted on a White/Spruiell orientation triangle.

Values of the biaxial orientation functions represented by eqs 1 are delimited by the boundaries of an isosceles triangle (Figure 2). Uniaxial orientation states with respect to the *x*, *y*, and *z* reference directions are denoted by the apices. Its altitude represents equal biaxial orientational states. Planar orientations ($\langle\cos^2\phi_{1x}\rangle = 0$) are situated along the base of the triangle, and isotropic systems are represented by the origin.

In crystalline systems, it is appropriate to define axis 1 as parallel to the normal of a crystalline plane. For orthorhombic crystal systems, where all three crystallographic axes *a*, *b*, and *c* are of varying lengths and are mutually perpendicular, one can rewrite eqs 1 as

$$F_{zj}{}^{B} = 2\langle\cos^2\phi_{jz}\rangle + \langle\cos^2\phi_{jy}\rangle - 1 \qquad (2a)$$

$$F_{yj}{}^{B} = 2\langle\cos^2\phi_{uy}\rangle + \langle\cos^2\phi_{jz}\rangle - 1 \qquad (2b)$$

where $j = a$, b, or c. In this case, only four of the resulting six crystalline orientation functions are independent.

Density. Two mixtures of isopropyl alcohol (ρ = 0.782 g/cm^3) and 99% diethylene glycol (ρ = 1.118 g/cm^3) having densities of 0.909 and 0.920 g/cm^3 were used to measure the density, *d*, of the blown film by simple flotation/submergence. The volume fraction of crystallinity, *X*, was consequently calculated by

$$X = \frac{(d - d_{am})}{(d_c - d_{am})} \tag{3}$$

where for PE, $d_c = 1.00$ g/cm^3 and $d_{am} = 0.855$ g/cm^3.[17]

Birefringence. The birefringence, Δ_{ij}, is defined as the difference in refractive index between two perpendicular directions i and j. It measures the global orientation (comprising crystalline, amorphous, and form effects) of the specimen. The following orientational states can be characterized by birefringence measurements upon a specimen using an orthogonal xyz reference system:

$$\Delta_{zx} = \Delta_{zy} = \Delta_{yx} = 0: \quad \text{isotropic system} \tag{4a}$$

$$\Delta_{zy} = \Delta_{zx} \text{ and } \Delta_{yx} = 0: \quad \text{uniaxial orientation along } z \tag{4b}$$

$$\Delta_{zx} = \Delta_{yx} > \Delta_{zy}: \quad \text{biaxial orientation in the } zy \text{ plane} \tag{4c}$$

The amount of amorphous orientation in the blown films can be estimated by assuming the simple two-phase model for PE. In this case, the total birefringence can be represented by

$$\Delta_{zx} = X(F_{zc}^{Bc}\Delta_{cb}^{oc} + F_{za}^{Bc}\Delta_{ab}^{oc}) + (1 - X)\Delta_{am}^{o}F_z^{Ba} + \Delta_f \tag{5a}$$

$$\Delta_{yx} = X(F_{yc}^{Bc}\Delta_{cb}^{oc} + F_{ya}^{Bc}\Delta_{ab}^{oc}) + (1 - X)\Delta_{am}^{o}F_y^{Ba} + \Delta_f \tag{5b}$$

where Δ_{cb}^{oc} and Δ_{ab}^{oc} are the intrinsic birefringences for the cb and ab planes of the unit cell, Δ_{am}^{o} is the amorphous intrinsic birefringence, F_z^{Ba} and F_y^{Ba} are the amorphous biaxial orientation functions, and Δ_f represents the contribution of the form birefringence.

Wide-Angle X-ray Diffraction (Pole Figures). Representation of the three-dimensional orientation of a crystalline plane can only be accomplished by using the pole figure technique. On a pole figure map, one may observe both the location and intensity of the orientation of a crystalline plane with respect to the x, y, and z reference directions. From the pole figure intensities of an (hkl) crystalline plane, it is possible to calculate the average squared cosine values of eqs 1. The evaluation of $\langle\cos^2 \phi_{hkl,z}\rangle$ with respect to the z reference axis can be carried out by

$$\langle\cos^2 \phi_{hkl,z}\rangle = \frac{\int_0^{\pi/2} I(\phi) \sin \phi \cos^2 \phi \, d\phi}{\int_0^{\pi/2} I(\phi) \sin \phi \, d\phi} \tag{6a}$$

where

$$I(\phi) = \int_0^{2\pi} I(\phi,\beta) \, d\beta \tag{6b}$$

In orientation studies, it is advantageous to know the orientation of the unit cell with respect to the reference directions, especially when different complex orientational state are present in a system (e.g., biaxial, double). If access to the orientational behavior of two of the crystallographic axes is possible (orthorhombic systems) by pole figure techniques, one may deduce the orientation of the third axis.

Experimental Section

Low-density poly(ethylene) (LDPE) having a density of 0.922 g/cm^3 and a melt index of 2.0 g/10 min kindly supplied by Dow Chemical Co. (sample no. 530C, lot no. CS165412). The beads were dried for a period of 6−8 h at 70 °C before performing the extrusion work.

All extrusion work was carried out at 200 °C. The polymer was introduced into a Killon-type single-screw ($\phi = 25$ mm) extruder turning at 51 rpm and was extruded through a 5.08 cm annular die possessing a 508 μm gap. Positioned immediately above the die of the blown film accessory is a circular hollow ring, which evenly distributes forced air on the outside surface of the blown tubular film. The velocity of this air exiting from the outlets was regularly adjusted by the deflector to stabilize the form of the bubble. The tubular film was held upright by a circular adjustable diaphragm and then gently collapsed by a series of guide rolls and the final nip rolls. The takeup speed (V_L) of the film after the nip rolls was measured by a tachometer and divided by the constant linear velocity (V_O) of the film tube exiting from the die to calculate the draw-down ratio (V_L/V_O). The blow-up ratio (B) was calculated by dividing the diameter of the bubble by that of the annular die. In series A, the blown film is subjected to an important increase in draw-down ratio from 1.9 to 7.9 for a low constant blow-up ratio of 1.68. In series B, the blow-up ratio of the blown film is gradually increased for six samples from 1.60 to 2.74 for a draw-down ratio held constant at 4.2. In both film series, bubble instability and/or rupture was prevented within the range of processing parameters given.

All birefringences of the blown film were measured by an Abbé refractometer (Bausch and Lomb, Model 3L) equipped with a polaroid. A mixture of α-chloronaphthalene (Anachemia) and silicon oil (Union Carbide R-850) having a refractive index of $n_D^{25} \approx 1.54$ was employed to eliminate the air/solid interface.

The X-ray radiation was produced by using a Rigaku generator (Rotoflex RU-200 BH) and emitted by a rotating Cu anode. Pole figure measurements were made by using nickel-filtered Cu Kα radiation produced at operating conditions of 55 kV and 195 mA. Collimation was induced by a series of Soller slits immediately followed by a vertical diffraction slit. Detection of the diffracted intensity was achieved by a scintillation counter coupled with a pulse-height analyzer. A semiautomatic pole figure assembly (Rigaku Model B-8) was secured upon the goniometer for pole figure measurements. Data collection was achieved by the software provided by Rigaku. Two experimental techniques are required to measure the intensities of eq 6b for a given Bragg angle θ: the Decker transmission method was used for $0° \le \alpha \le 75° - \theta$ (N.B., $\alpha = 90° - \phi$), while the Schultz reflection method was employed for the remaining α values up to and including 90°. For the Decker transmission method, the width of the diffraction slit was 0.1 mm. However, for the Schultz reflection technique, the width of the diffraction slit was varied from 0.5° for the (200) plane to 1° for the (020) diffraction plane. In this case, height and width delimiting slits were also necessary. The widths of the receiving and scattering slits for both methods were 4 and 5 mm, respectively, for all films and planes investigated. An angle step of 5° for α and β was used during the measurements. A pole figure data processing program written by us was employed to correct the raw data and to calculate the average squared cosine values of the angles $\phi_{hkl,k}$ with respect to the machine, transverse, and normal reference directions of the sample. Correction for background and absorption effects, the connection of the two experimental methods, and a nine-point data smoothing process were performed before plotting the pole figures.

The (002) pole figure was unmeasurable due to the low degree of crystallinity of the films and due to interference from other crystalline planes that diffract at the same Bragg angle. The strong (110) diffraction peak ($2\theta = 21.4°$) was largely affected by the broad amorphous halo ($2\theta = 19.2°$), and, hence, was not used for quantitative analysis. As PE possesses an orthorhombic unit cell, quantitative values of $\langle\cos^2 \phi_{ck}\rangle$ have been calculated by means of $\langle\cos^2 \phi_{ak}\rangle$ and $\langle\cos^2 \phi_{bk}\rangle$.[18]

Nickel-filtered Cu Kα radiation generated at 50 kV and 190 mA was employed to investigate X-ray scattering effects at small angles. Collimation of the X-ray beam was achieved by using a series of four pinholes: $\phi_1 = 0.3$, $\phi_2 = 0.15$ (height adjusting; $d_{12} = 10.0$), $\phi_3 = 0.15$ ($d_{13} = 21.0$), and $\phi_4 = 0.20$

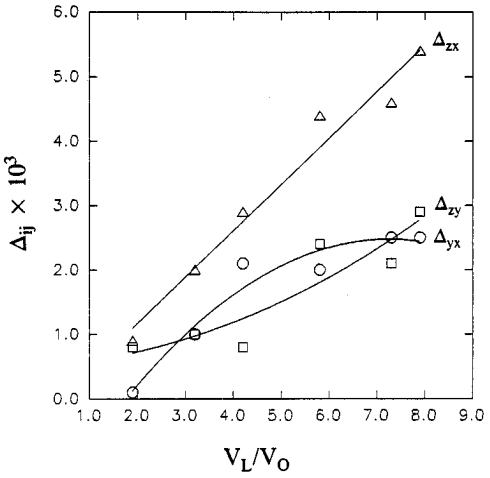

Figure 3. Birefringence as a function of draw-down ratio for the films of series A ($B = 1.68$).

($d_{14} = 29.8$), where the ϕ_i's are the diameters (millimeters) of the pinholes and the d_{ij}'s refer to the distance (centimeters) between pinholes 1 and j. The photographic plate within the Rigaku-denki camera was located 38.2 cm from the sample, which was securely positioned upon pinhole 4. Contrary to the wide-angle work, where single films were used, films were carefully stacked together to give sample thicknesses of roughly 2−3 mm to enhance the intensity of the scattering. Photographs of the small-angle scattering were taken along the ND, TD, and MD so as to probe the structure of the morphology contained within the blown films. Exposition times varied from 12 to 24 h.

Results and Discussion

Figure 3 illustrates the variation of the birefringence as a function of draw-down ratio for the blown films of series A. All birefringence values have a maximum error of 0.0005. For the first sample, we note that $\Delta_{zx} = \Delta_{zy}$ and $\Delta_{yx} = 0$, satisfying eq 4b and signifying that the film contains a global orientation that is uniaxial about the MD. Increases in the draw-down ratio cause the loss of this initial uniaxial orientation, as we observe for all films that $\Delta_{zx} > \Delta_{zy} \approx \Delta_{yx}$. The birefringence in the zx plane increases linearly with draw down. The Δ_{zy} birefringence varies gradually in value and increases to approximately 0.0028 for higher draw downs. The third birefringence, Δ_{yx}, increases slowly and levels off toward a value of 0.0025. Uniaxial orientation states were not retained upon increasing the draw-down ratio. These results are comparable to those of Choi *et al.*,[13] who witnessed the same birefringence trend for increasing draw down at a constant blow-up ratio with HDPE, except for the fact that Δ_{zy} was greater than Δ_{yx}.

Figures 4 and 5 present the pole figure results for three LDPE films of the A series having draw-down ratios of 1.9, 4.2, and 7.9 for a constant blow-up ratio of 1.68. By glancing at the (200) pole figures in Figure 4, it is evident that the a axis is preferentially oriented along the machine direction in all films. The magnitude of the orientation increases with the draw-down ratio, as seen by the increase in concentration of contour intensity lines about the MD for the last sample. The b axis orientation, given by the (020) pole figures of Figure 5, is also seen to vary with the draw down. For low draw-down ratios, it is situated normal to the film plane, but for higher draw downs, it tends to orient in the ND, TD plane, keeping, however, a strong orientation component along the ND.

The White/Spruiell orientation functions plotted on the orientation triangle of Figure 6 graphically illustrate

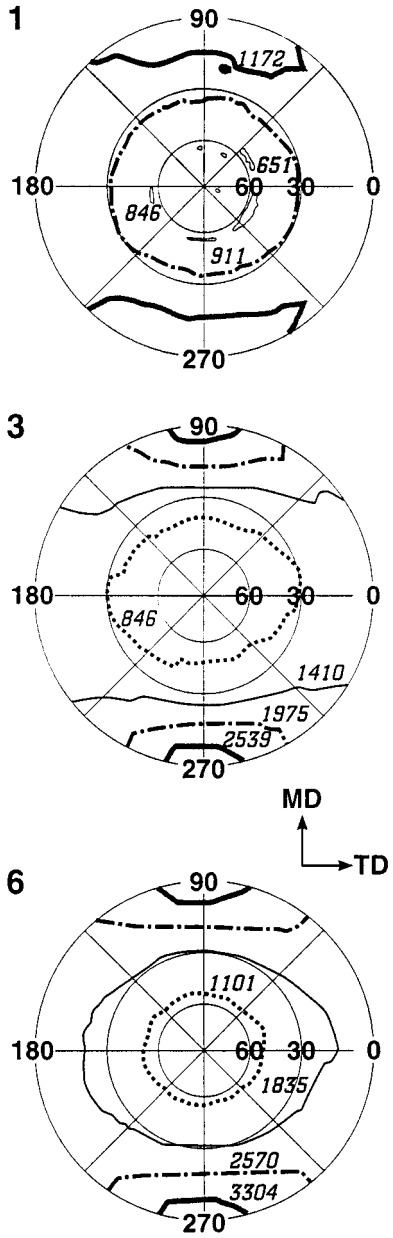

Figure 4. Pole figures (200) for films 1, 3, and 6 of series A. The isotensity lines are drawn in order of decreasing intensity. For example, for film 3, the thick continuous line ($I = 2539$) refers to the highest intensity, followed by the dashed line ($I = 1975$), the thin continuous line ($I = 1410$), and the dotted line ($I = 846$). The intensity value is always indicated next to the corresponding line.

the orientation observed on the pole figures. The three orientation points of sample 1 lie on the dashed biaxial orientation line, indicating, although weakly, that an equal biaxial orientation is present in the crystalline regions. Upon increasing the draw-down ratio, only the successive orientation points for the a axis seem to vary linearly, while the other points do not possess good correlated behavior with draw down. In spite of this, the orientation points generally move away from the broken line. The calculated c axis orientation distribution seems to suggest that the molecular chains retain equal biaxial behavior in all of the films. In summary, by way of the behavior of the a and b axes, it is evident that the general a axis orientation becomes increasingly defined with draw down and more oriented along the machine direction.

SAXS photographs of the three blown films characterized in series A by the pole figure analysis are

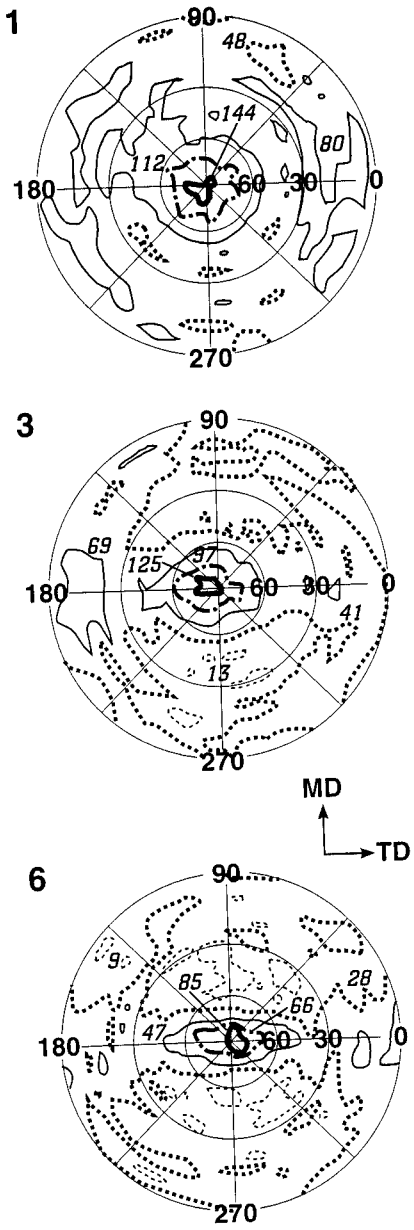

Figure 5. Pole figures (020) for films 1, 3, and 6 of series A. The intensity code is the same as in Figure 4.

presented in Figure 7. A complete halo is observed around the beam stop for the sample of lowest draw down (film 1), no matter what the direction of the impinging X-ray beam. The scattering patterns are typical of a sample containing a lamellar morphology. However, given the crystal orientation as shown by the pole figures in Figures 4 and 5, the strong *b* axis orientation along the ND suggests that a substantial amount of transcrystalline material is present in the film. Numerous nucleating sites along the film surface, as well as rapid cooling of the polymer melt, have been proven to promote this morphology in blown films. Due to the proximity of the nucleating centers, the full development of the spherulites is impeded, forcing the lamellar growth direction along the film normal.[5,10] A simple illustration showing the deposition of the lamellae of the transcrystalline layer on the film surface is illustrated in Figure 8. Given the fact that the *b* axis of PE is parallel to the growth direction of the lamellae, the (020) pole figure should display high orientation along the ND. Consequently, the *a* and *c* axes are oriented preferentially in the film plane. These criteria

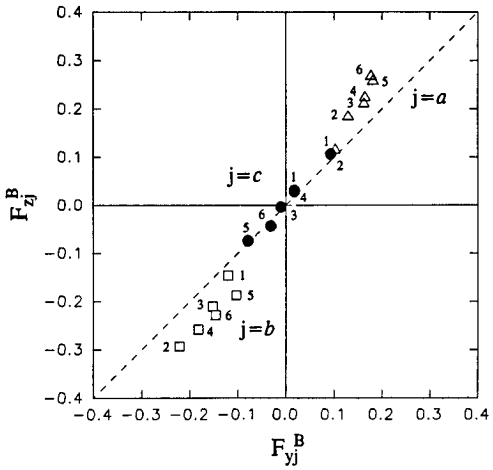

Figure 6. Crystalline orientation behavior of the films of series A (sample 1, $V_L/V_O = 1.9$; 2, $V_L/V_O = 3.2$; 3, $V_L/V_O = 4.2$; 4, $V_L/V_O = 5.8$; $V_L/V_O = 7.3$; 6, $V_L/V_O = 7.9$.

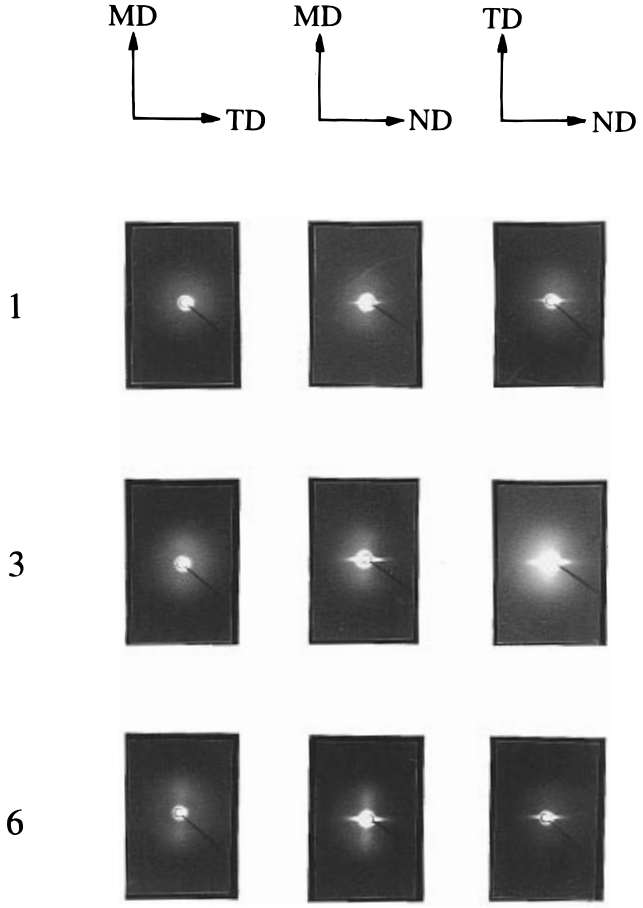

Figure 7. SAXS patterns of films 1, 3, and 6 of series A taken with the X-ray beam passing through the normal, transverse, and machine directions.

are met in the case of film 1 and prove the existence of an important transcrystalline layer in the film's superstructure. The weak *a* axis orientation along the MD, however, suggests that a small proportion of Keller/Machin 1 row-nucleated morphology is present in the bulk.

As the draw-down ratio is increased (no. 3), the strong halo remains for the X-ray beam directed along the ND. However, along with a weak halo, a two-point diagram seems to manifest itself in the image taken along the TD. Despite the possible overexposition, the third diagram of this series shows substantial scattering

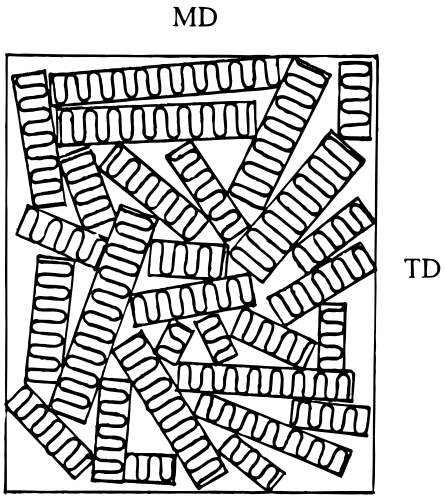

Figure 8. Simple schema depicting the film surface of a blow film containing a transcrystalline morphology. Growth direction of the lamallae is into the paper along the ND.

around the beam stop. The two-point diagram along the MD suggests that a larger proportion of row-nucleated morphology has been generated in the bulk. This is also suggested by the increase in *a* axis orientation along the MD on the corresponding pole figure. An important transcrystalline morphology, however, still exists within the film.

For the highest drawdown ratios (no. 6), major developments in the small-angle scattering are observed. A weak halo and a two-point diagram along the MD for the X-ray beam perpendicular to the film surface are seen in the first photograph. When the beam is directed along the TD, a strong two-point diagram oriented toward the MD is manifest. In the final SAXS pattern, weak scattering can be observed along the transverse direction. With the predominance of the two-point diagrams along the MD, and the strong *a* axis orientation along this same direction, the morphology has become primarily row-nucleated in nature. Some transcrystalline material is still present, as indicated by the weak halo seen in the first image of the series. Higher stress in the melt, caused by increasing the draw-down ratio, seems to promote row nucleation at the expense of the transcrystalline morphology. Furthermore, the crystal orientation within the row-nucleated morphology follows the Keller/Machin 1 model, indicating that the stresses were not high enough to promote their second morphological model.

The density of all blown films was found to vary little with the processing conditions, and the measured values were considered constant at 0.916 g/cm^3, giving a degree of crystallinity of 46% by eq 3. By inserting this value along with the biaxial crystalline orientation functions, birefringence values, and $\Delta_{cb}^{oc} = 0.056$, $\Delta_{ab}^{oc} = -0.005$, and $\Delta_{am}^{o} = 0.058$[19] into eqs 5, it was possible to infer the orientation behavior of the amorphous regions with draw-down ratio by assuming no contribution from form effects. This variation is presented in Figure 9. The initial films, 1 and 2, have orientation values near zero, but an increase in draw down causes the orientation factors to increase simultaneously, with the general trend that $F_z^{Ba} > F_y^{Ba}$. A certain amount of general biaxial orientation has been induced in the amorphous regions, but it is unbalanced in the film plane as it appears stronger along the extrusion than the transverse direction.

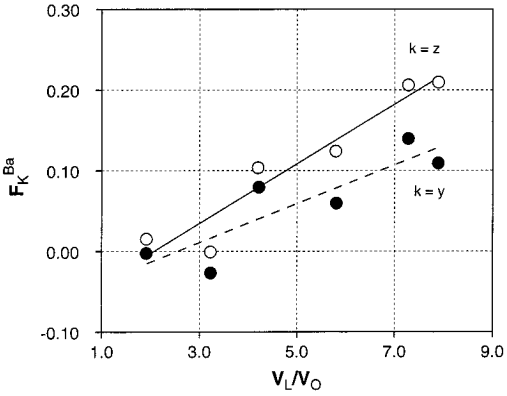

Figure 9. Amorphous orientation behavior as a function of draw-down ratio for the films of series A ($B = 1.68$).

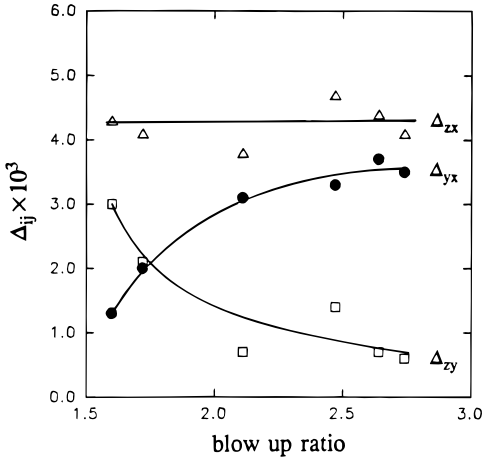

Figure 10. Birefringence as a function of blow-up ratio for the blown films of series B ($V_L/V_O = 4.2$).

Figure 10 presents the variation of the birefringence as a function of blow-up ratio for the blown films of series B. As intuitively expected, the Δ_{yx} birefringence increases to the detriment of Δ_{zy}, which, in turn, diminishes to low birefringence values near 0.0006. It is striking to note the relatively constant birefringence values in the *zy* plane with increasing blow-up ratio ($\Delta_{zx} \approx 0.0043$). For a constant draw-down ratio of 4.2, we observe that the overall global orientation remains constant in the *zx* plane. Enlargement of the bubble diameter dramatically increased the global orientation in the *yx* plane to values approaching those in the *zx* plane. According to eq 4c, we can conclude that, globally, the orientation approaches biaxial behavior for samples beyond blow-up ratios of approximately 2.5.

The (200) and (020) pole figures for the samples of the B series possessing blow-up ratios of 1.60, 2.47, and 2.74 are presented in Figures 11 and 12, respectively. The (200) pole figure of the initial sample indicates the presence of an *a* axis orientation along the MD in the crystalline regions. However, upon increasing the blow-up ratio to 2.47, a substantial increase in orientation develops in the MD/TD plane. Finally, for higher blow-up ratios, we notice that this planar orientation develops intensity maxima roughly between the machine and transverse reference directions of the pole figure. Lindenmeyer and Lustig[4] observed a similar development of the (200) orientation upon increasing the blow-up ratio in LDPE, culminating in a unique planar *a* axis distribution at high blow ups. The highest blown LDPE sample of Ashizawa *et al.*[7] borders uniplanar *a* axis orientation, but a strong orientation component remains

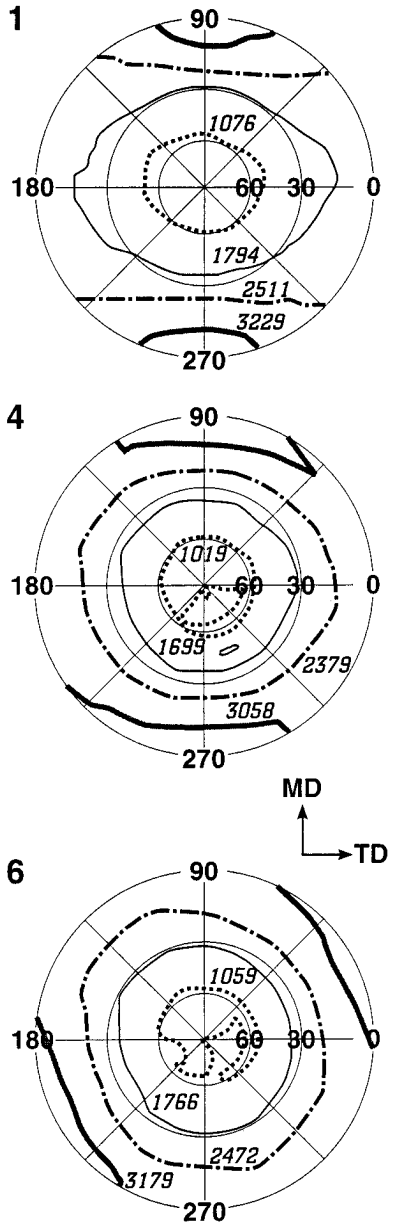

Figure 11. Pole figures (200) of films 1, 4, and 6 of series B. The intensity code is the same as in Figure 4.

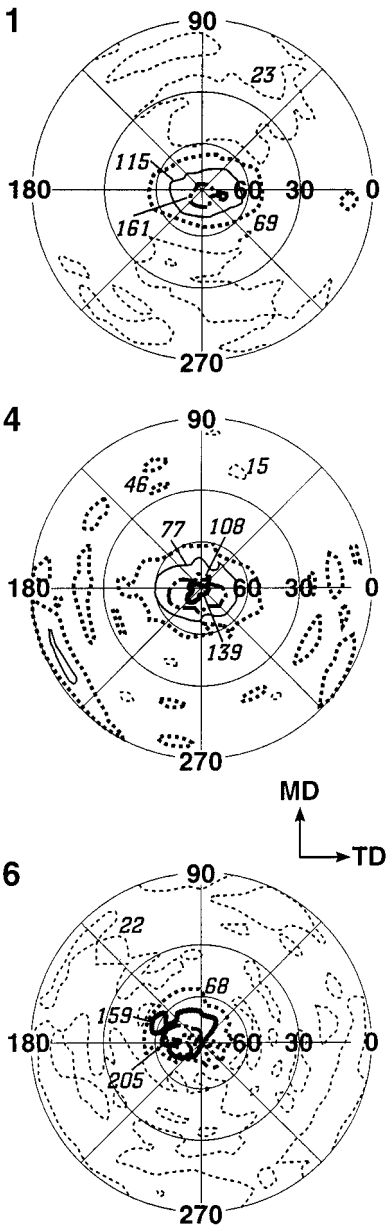

Figure 12. Pole figures (020) of films 1, 4, and 6 of series B. The intensity code is the same as in Figure 4.

along the MD in their films. The (020) plane orientation varies little with the blow-up ratio and remains, for all intents and purposes, oriented with its normal perpendicular to the film surface. The strong tendency of the *b* axis to align along the ND in highly blown LDPE film has been seen in other extrusion studies.[4,8] This overall behavior suggests that only the *a* and *c* crystallographic axes are experiencing reorientation upon increasing the blow-up ratio.

The orientation diagram of Figure 13 confirms the conclusions deduced from the pole figures. All film samples contain a degree of equal biorientation in the crystalline regions due to their proximity to the broken biaxial orientation line. Particularly, we note that the initial *a* axis orientation along the MD slowly becomes equally bioriented with respect to the MD and the TD. Sample 6 is equal biaxially oriented according to the White/Spruiell orientation functions.

The effect of increasing the blow-up ratio on the appearance of scattering at small angles is presented in Figure 14 for films 1, 4, and 6 of series B. For film 1, with the X-ray beam directed along the ND, a complete halo as well as a two-point diagram in the MD is observed. The same pattern is observed along the TD, except for the fact that the two-point diagram appears to be stronger. A very weak halo around the beam stop is apparent when the beam is projected in the MD. Given the combination of weak halos and two-point diagrams, film 1 of this series contains both the transcrystalline and row-nucleated morphologies. The strong *b* axis orientation in the ND and the preferential orientation of the *a* axis along the MD from the pole figure results confirm these deductions.

Increases in the blow-up ratio cause important changes with respect to the morphology. A strong halo is dominant in the MD,TD plane. A combination of a two-point diagram along the MD with a weak halo is observed when the X-ray beam is directed in the TD. For the last photo of the series, scattering is observed primarily along the TD. On account of these three SAXS scattering patterns, we believe to have induced a morphological distribution that has been proposed for biaxially oriented PE prepared by the tubular film process.[13] Application of a balanced biaxial stress in

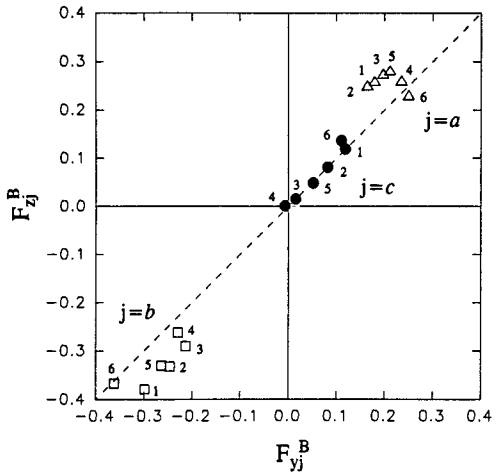

Figure 13. Crystalline orientation behavior of the films of series B (sample 1, $B = 1.60$; 2, $B = 1.72$; 3, $B = 2.11$; 4, $B = 2.47$; 5, $B = 2.64$; 6, $B = 2.74$).

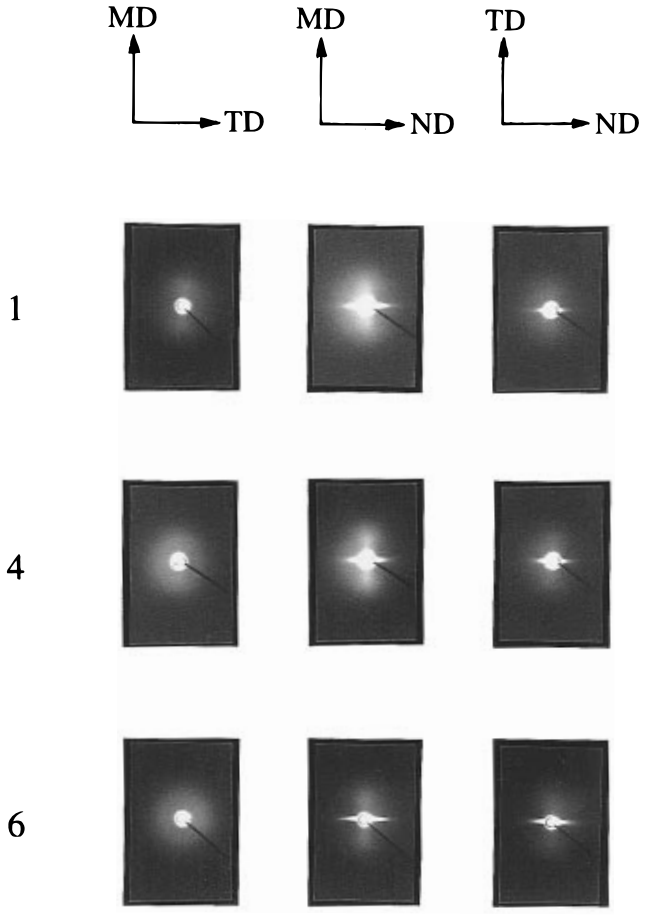

Figure 14. SAXS diagrams of films 1, 4, and 6 of series B.

the MD,TD plane of the bubble would force intuitively the chain bundles and extended chains to become isotropically distributed in the plane of the polymer melt. Upon cooling, crystallization would occur along these radially oriented nucleating agents, thus causing the resulting row morphology to be uniformly distributed in the MD,TD plane of the polymer film, as illustrated in Figure 15. This morphological distribution conceivably would give corresponding (200) and (020) pole figures of the last example of Figures 11 and 12, as the (020) pole figure of Figure 1a, averaged about the ND, gives a maximum *b* axis orientation along the ND. Some transcrystalline material is still present due

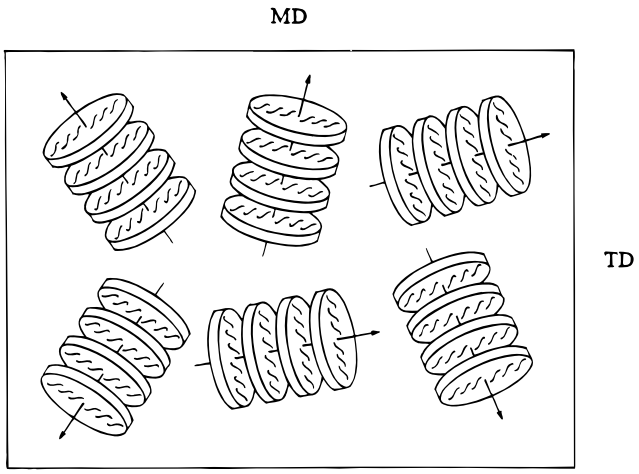

Figure 15. Distribution of the row-nucleated morphology in biaxially oriented LDPE films. (N.B., It is restricted to the film plane, but its *a* axis orientation is randomized in the same plane.)

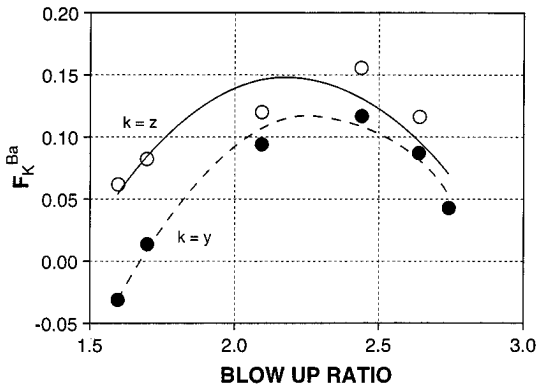

Figure 16. Amorphous orientation behavior as a function of blow-up ratio for the series B films ($V_L/V_O = 4.2$).

to the weak halo, as seen when the X-ray beam is passed by the TD.

For the film of highest blow-up ratio, SAXS patterns similar to those in the prior film sample are observed. To summarize the three photographs, a strong halo and an important two-point diagram along the MD and along the TD are apparent when the X-ray beam is directed through the ND, TD, and MD. In film 6, the planar distribution of the Keller/Machin 1 morphology is even more apparent. The amount of transcrystalline material seems to have lessened proportionately. To summarize, increases in the blow-up ratio for constant draw downs gradually distribute the Keller/Machin 1 morphology equally within the film plane.

Figure 16 presents the amorphous orientation behavior as a function of blow-up ratio for all films of series B, as calculated by eq 5. Three different orientation behaviors can be interpreted from this diagram. First, the predominance of F_z^{Ba} over F_y^{Ba} suggests uniaxial behavior for low blow-up ratios. There is, however, a tendency toward biaxial orientation for intermediate blow-up ratios, but it is unbalanced as F_z^{Ba} is still slightly greater than F_y^{Ba}. Finally, at higher blow-up ratios, an equal biaxial orientation, albeit weak, has been induced in the amorphous regions due to the superposition of both orientation values.

We now are in a position to correlate the results of both film series by means of sample 3 of series A ($V_L/V_O = 4.2$, $B = 1.68$) and sample 2 of series B ($V_L/V_O = 4.2$, $B = 1.72$), given their similar processing history.

Table 1. Summary of the Orientation and Morphologies Induced in the Blown LDPE Film of Series A

region	low draw down	high draw down
crystalline	weak *a* axis orientation along the MD	stronger *a* axis orientation along the MD
amorphous	isotropic	toward biaxial
cryst + amorph	uniaxial along the MD	less uniaxial
morphology	transcrystalline ↑ and Keller/Machin 1	Keller/Machin 1 ↑ and transcrystalline

Table 2. Summary of the Molecular Orientation and Morphologies in the Blown Films of Series B

region	low blow-up ratios	high blow-up ratios
crystalline	*a* axis orientation along the MD	*a* axis orientation in the MD,TD plane
amorphous	uniaxial along the MD	equal biaxial in film plane
cryst + amorph	undefined	biaxial
morpholgy	transcrystalline + Keller/Machin 1	Keller/Machin 1 in the MD,TD plane

In both cases, an important *a* axis orientation along the MD is present in the crystalline regions, with comparable orientation function values (Figure 6 and 13). We also note that the amorphous orientation presented for both samples has similar magnitudes along the extrusion direction (Figures 9 and 16). However, sample 3 of series A shows biaxial behavior in the film plane compared to an uniaxial amorphous orientation in series B. The origin of the difference between the amorphous orientation for these two samples is unknown, but it must be realized that other processing parameters may heavily affect orientation in the tubular film. Besides the draw-down and blow-up ratios and the constant extruding conditions, the cooling rate of the film bubble regulated by the velocity of forced air applied to the exterior of the molten film influences the crystallization kinetics and the resulting orientation in tubular film.[5,10,19] The anomaly observed in the above-mentioned amorphous orientation, as well as the discrepancy between successive orientation points as in Figures 6 and 13, is most likely explained by this effect. In our study, the cooling rate velocity was regularly adjusted to promote bubble stability. LDPE is prone to bubble instability upon any increase in takeup speed, as noted by Han and Park.[20] Variation of the surface temperature of the film during processing can also influence molecular orientation and the uniformity of final properties of the film plane.[21] As a general rule, molecular orientation is highly sensitive to all external factors used in producing tubular film. Inconsistencies between successive orientation measurements on a film series are likely if more than one parameter has been changed at a time. Hence, molecular orientation measurements on a series of film, important to infer end-use properties, are doubly important for verifying the consistency of the processing conditions.

Table 1 summarizes the molecular orientations observed in the crystalline, amorphous, and crystalline + amorphous regions, as well as the morphology in the blown films of series A as a function of draw down. At low draw-down ratios, an important transcrystalline morphology with a smaller amount of Keller/Machin 1 row nucleation exists in the bulk of the films. The crystalline regions are surrounded by an isotropic amorphous matrix. Globally, the orientation is prevalent along the extrusion direction. Upon increasing the draw-down ratio, the *a* axis orientation increases its definition along the MD, thus indicating retention of the type 1 morphology. Less transcrystalline material is present at higher draw downs. Similar results were reported by Desper[5] on LDPE film by increasing the cooling rate velocity for constant blow-up and draw-down ratios. In our study, the stresses applied in the polymer melt were not sufficient to cause the appearance of the type 2 morphology, in which the *c* axis is oriented along the MD. This transition has been induced in HDPE by using slower cooling conditions, which, consequently, translates into higher freeze-line heights.[11] Under similar processing conditions with HDPE, Choi *et al.*[13] observed that the *a* axis toppled from the MD at higher draw downs, thus generating an intermediate Keller/Machin morphology. Last, the amorphous regions did not develop a uniaxial orientation along the MD due to the appearance of a strong orientation component along the TD. Negative amorphous orientation values have been reported for a similar series of HDPE films, indicating that the molecular chain axes are normal to the film surface in the amorphous regions.[13]

The molecular orientation and morphologies induced in the blown films of series B upon increasing the blow-up ratio are presented in Table 2. The initial films contain a combination of Keller/Machin 1 and transcrystalline morphologies. The amorphous regions, as the oriented rows, have a tendency to be uniaxially aligned along the extrusion direction. However, upon increasing the blow-up ratio to maximum values, biaxial orientation states were induced in all structural levels of PE. The pole figure of the (200) plane clearly shows that the *a* axis has become strongly oriented in the film plane. This particular orientation of the PE unit cell, having the molecular chains aligned isotropically within the film plane, is best described as uniplanar by using the notation of Heffelfinger and Burton.[22] This unique orientational behavior of LDPE has been observed by pole figure analysis with a reference to Keller/Machin's model of row nucleation.[4,7] The row-nucleation morphology dominates the superstructure and is oriented preferentially in the film plane, as depicted in Figure 15.

Bubble rupture occurred when the blow-up ratio was increased beyond 2.74 for a constant draw-down ratio of 4.2. Intuitively, the orientation of the row-nucleated morphology would have been enhanced along the transverse directions, more than likely attenuating the uniplanar orientation. It is probable that such molecular orientation situations create instability in LDPE tubular film processing and, therefore, should be avoided at all costs.

The molecular chains in the amorphous regions of series B between the rows and bundles are oriented biaxially. More precisely, it is likely that these regions are oriented in the film plane due to the well-defined orientation of the crystalline regions. This contrasts with work containing similar crystalline orientation,[7] in which the molecular chains in the amorphous regions were found to orient themselves normal to the film surface.

Conclusions

All LDPE films prepared by the tubular film process were found to contain a mixture of Keller/Machin 1 and transcrystalline morphologies. In a first set of films (series A), in which the draw-down ratio was increased for a constant blow-up ratio of 1.69, the amount of row nucleation increased to the detriment of the transcrystallization. The row-nucleated structures became more defined along the machine direction. This is apparent from the dramatic increase in the pole density of the *a* axis along the MD, as shown on the (200) pole figure. The appearance of two-point diagrams along the MD on the SAXS patterns confirms this conclusion. The amorphous regions, presenting little orientation at first, acquire a slight biaxial orientation according to the orientation function analysis.

For a second set of LDPE films (series B), where the blow-up ratio was increased for a constant draw-down ratio of 4.2, the row-nucleated morphology, weakly aligned on the onset along the MD, becomes progressively oriented in the film plane upon transverse stretching. The *a* axis, as well as the molecular chains, is aligned in this same plane due to the strong orientation of the *b* axis along the ND. The amount of transcrystalline material steadily decreases upon increasing the blow-up ratio. The crystalline regions are best described as containing a uniplanar orientation. For the highly blown films, the amorphous regions were also characterized as biaxially oriented by the orientation functions, most likely signifying the same uniplanar orientation of the crystalline regions.

Finally, the importance of controlling the experimental parameters used in tubular film production is underlined. The cooling rate velocity, for example, can greatly influence orientation results and, thus, final general properties of the blow film. Molecular orientation is highly sensitive to the processing conditions and, thus, can be used as an aid to verify their consistency during film production.

Acknowledgment. The authors thank Mr. C. P. Lafrance for writing the pole figure data processing program, the National Research Council of Canada for use of the extruder/blown film unit at the Industrial Materials Research Institute (Boucherville, Québec), Mr. C. de Grandpré of this institute for aiding in the preparation of the blown films, Mr. G. Plante for the SAXS photoreproductions, Dr. A. Ajji for his useful suggestions, and, finally, NSERC and the Department of Education of the Province of Québec (Fonds FCAR and Action Structurante) for their financial support.

References and Notes

(1) White, J. L.; Cakmak, M. Orientation Processes. In *Encyclopedia of Polmer Science and Engineering*; Mark, H., Bikales, N. M., Overberger, C., Menges, G., Eds.; Wiley-Interscience: New York, 1987, Vol. 10, p 619.
(2) DeVries, A. J.; Bonnebat, C.; Beautemps, J. *J. Polym. Sci.: Polym. Symp.* **1977**, *58*, 109.
(3) Keller, A.; Machin, M. J. *J. Macromol. Sci. (Phys.)* **1967**, *B1*, 41.
(4) Lindenmeyer, P. H.; Lustig, S. *J. Appl. Polym. Sci.* **1965**, *9*, 227.
(5) Desper, C. R. *J. Appl. Polym. Sci.* **1969**, *13*, 169.
(6) Haudin, J. M. *Ann. Chim. Fr.* **1980**, *5*, 513.
(7) Ashizawa, H.; Spruiell, J. E.; White, J. L. *Polym. Eng. Sci.* **1984**, *24* (13), 1035.
(8) Walenta, E.; Janke, A.; Hofmann, D.; Fanter, D.; Geiss, D. *Acta Polym.* **1986**, *37* (9), 557.
(9) Kwack, T. H.; Han, C. D.; Vickers, M. E. *J. Appl. Polym. Sci.* **1988**, *35*, 363.
(10) Maddams, W. F.; Preedy, J. E. *J. Appl. Polym. Sci.* **1978**, *22*, 2721.
(11) Maddams, W. F.; Preedy, J. E. *J. Appl. Polym. Sci.* **1978**, *22*, 2739.
(12) Maddams, W. F.; Preedy, J. E. *J. Appl. Polym. Sci.* **1978**, *22*, 2751.
(13) Choi, K. J.; Spruiell, J. E.; White, J. L. *J. Polym. Sci., Polym. Phys. Ed.* **1982**, *20*, 27.
(14) Maddams, W. F.; Vickers, M. E. *J. Elast. Plast.* **1983**, *15*, 246.
(15) Kobayashi, K.; Nagasawa, T. *J. Polym. Sci.: Part C* **1966**, *15*, 163.
(16) White, J. L.; Spruiell, J. E. *Polym. Eng. Sci.* **1981**, *21*, 859.
(17) Pazur, R. J.; Prud'homme, R. E. *J. Polym. Sci. Polym. Phys. Ed.* **1994**, *32*, 1475.
(18) Desper, C. R.; Stein, R. S. *J. Appl. Phys.* **1966**, *37*, 3990.
(19) Harris, W. D.; Van Kerckhoven, C. A. A.; Cantu, L. K.; *J. Plast. Film. Sh.* **1990**, *6*, 306.
(20) Han, C. D.; Park, J. Y. *J. Appl. Polym. Sci.* **1975**, *19*, 3291.
(21) Karande, S. V.; Chum, S. P.; Huang, W. L. *J. Plast. Film. Sh.* **1992**, *8*, 74.
(22) Heffelfinger, C. J.; Burton, R. L. *J. Polym. Sci.* **1960**, *47*, 289.

MA9464229